Interfacial Phenomena and Heat Transfer, 2 (3): 273–292 (2014)

EMPIRICAL AND MODELING-BASED CORRELATIONS FOR POOL BOILING ON MICROSTRUCTURED SURFACES

E. Teodori, A. S. Moita,* & A. L. N. Moreira

Center for Innovation, Technology and Policy Research, Instituto Superior Tecnico, Universidade de Lisboa, Av. Rovisco Pais, 1049-001 Lisboa, Portugal

*Address all correspondence to A. S. Moita, E-mail: anamoita@dem.ist.utl.pt

This paper proposes new correlations to predict the pool-boiling heat transfer coefficients on micropatterned silicon wafer surfaces. Two different approaches were followed in this study. The first approach consisted of developing a modified Rohsenow correlation, which includes a geometrical parameter that can accurately describe the topology of the surfaces. In the second approach, original correlations were devised based on a dimensional analysis. The independent data required for validation of the proposed relations were collected by coupling high-speed visualization and image postprocessing with heat flux/surface temperature measurements. Additional data were taken from the literature, for comparative purposes. The modified Rohsenow correlation was able to predict the pool-boiling heat transfer coefficients for all of the fluid/surface combinations tested (which were gathered with additional data reported in the literature) within an error of ±20%. The two correlations obtained by dimensional analysis were slightly different in terms of the phenomenological description of the boiling process. Both were able to predict the heat transfer coefficient within an error of ±30%. In addition, these correlations could predict the behavior of fluids with significantly different thermophysical properties. The main difference between the relations proposed here is that, while the first correlation, based on Rohsenow's approach, can only partially capture the mechanisms involved in the pool-boiling process, the second approach provides a dimensional analysis based on the heat flux partitioning model widely known in literature, which seems to be more representative of the governing mechanisms.

KEY WORDS: *pool-boiling heat transfer, microstructured surfaces, heat removed by quenching, surface topography, surface topology, empirical correlation*

1. INTRODUCTION

In the context of cooling techniques for electronic components, direct immersion in a boiling dielectric fluid has been shown to be extremely efficient in removing high thermal loads from electronic components at low values of wall superheat. Considering that the working temperatures of most electronic components are relatively low (on the order of 0–85°C), the working fluid must have a low saturation temperature at atmospheric pressure. For safety reasons, the fluid must also be dielectric. Unfortunately, fluids with such characteristics also exhibit lower values of thermophysical properties that are relevant to heat transfer processes (e.g., latent heat of evaporation and specific heat) when compared with other common fluids such as ethanol or water. To tackle this issue one can enhance the cooling performance by microstructuring the surface.

Electronic chips are often simulated using silicon wafers. In this context, different geometrical arrangements are proposed in the literature (e.g., Anderson and Mudawar, 1989; Honda et al., 2002). Several authors report that etched cavities on wafer surfaces are efficient in increasing pool-boiling heat transfer coefficients. For instance, Yu et al. (2006) reported an increment in the heat transfer coefficient as high as 150% for the boiling of FC 72 on surfaces micropatterned with circular cavities of diameters ranging 50–200 μm and depths of 110–200 μm. The authors varied the distance between cavities 100–400 μm. Nitesh et al. (2006) reported an increment in the heat transfer coefficient

2169-2785/14/$35.00

NOMENCLATURE

a	side length of the square cavities composing micropatterns on silicon surfaces (m)
$a1$	fitting constant (-)
$a2$	fitting constant (-)
$a3$	fitting constant (-)
$a4$	fitting constant (-)
A_{en}	liquid-solid contact area of the structured surfaces (m^2)
A_{smooth}	liquid-solid contact area of the smooth surfaces (m^2)
b	fitting constant (-)
C	fitting constant (-)
C_{sf}	fitting parameter of the Rohsenow correlation (-)
Cp_l	specific heat of the liquid [kJ/(kgK)]
g	gravity acceleration (m/s^2)
h	heat transfer coefficient [$W/(m^2K)$]
h_{av}	average heat transfer coefficient on a microstructured surface [$W/(m^2K)$]
h_{fg}	latent heat of evaporation (kJ/kg)
h_R	depth of the square cavities composing the micropatterns on the surfaces (m)
h_{smooth}	average heat transfer coefficient on a smooth surface [$W/(m^2K)$]
k_l	thermal conductivity of the liquid [W/(m.K)]
L_c	capillary length representing the bubble departure diameter (m)
m	exponent of the Rohsenow correlation (-)
n	exponent of the Rohsenow correlation (-)
Pr_l	Prandtl number of the liquid phase (-)
q	dimensional variables in the Buckingham (pi) theorem (-)
q''	heat flux (W/m^2)
Re_b	Reynolds number for the bubble departure diameter, as defined in the Rohsenow correlation (-)
r_f	roughness factor (-)
S	distance between the square cavities composing the micropatterns on the silicon surfaces (m)
St^*	modified Stanton number as defined in the Rohsenow correlation (-)
T_{sat}	saturation temperature (K)
t_b	characteristic time between the departure of consecutive bubbles (s)
ΔT	Wall superheat (K)
V	velocity (m/s)

Greek Symbols

θ	equilibrium contact angle
μ_l	dynamic viscosity of the liquid (Nm/s^2)
ν_l	kinematic viscosity of the liquid (m^2/s)
Π	pi group in the Buckingham (pi) theorem (-)
ρ_l	density of the liquid (kg/m^3)
ρ_v	vapor density (kg/m^3)
σ_l	surface tension of the liquid (N/m)
Φ	functional relationship among pi groups (-)

Acronyms

fps	frame per second
PID	proportional integrative derivative
PIV	particle image velocimetry

Subscripts

l	liquid
v	vapor
sat	saturation
b	bubble diameter
sf	solid-fluid
R	roughness
$smooth$	smooth surface
av	average
en	enhanced

of 50% for the pool boiling of FC 72 on surfaces micropatterned with pyramidal cavities of mouth dimensions of 40μm and base dimensions of 240 μm. The spacing between the cavities was varied 500–1,000 μm.

Despite such encouraging results, there is still no agreement in the literature concerning the optimal micropatterns for maximizing pool-boiling heat transfer. This is understandable given the high sensitivity of such studies to the

particular applications and working conditions that are being considered. A methodology is desired to avoid the trial-and-error approach that has been used so far. Recognizing the need to fix the geometry of the cavities, and after some preliminary work in which the shape and basic size of the cavities were investigated, Moita et al. (2012) and Teodori et al. (2013) studied the boiling of water, ethanol, and HFE 7000 on micropatterned surfaces with square cavities of fixed dimensions (the side length of the square was a = 52 μm and the depth of the cavities was h_R = 20 μm). The only quantity that was changed was the distance between cavities, S, which was varied 300–1,200 μm. The authors observed an increment in the heat transfer coefficients as high as 150% and discussed the relevance of the distance between cavities in such enhancement.

The most obvious reasons for the increase in the heat transfer coefficient in pool boiling on microstructured surfaces, as reported in the various aforementioned studies, are the surface enhancement in terms of the increase in the fluid/surface contact area and the increase in the number of cavities, which are more likely to act as nucleation sites and thus promote the heterogeneous nucleation process. However, it would be extremely simplistic to consider that these two parameters linearly affect the heat transfer coefficients. In fact, Yu et al. (2006), Nitesh et al. (2006), Moita et al. (2012), and Teodori et al. (2013) observed that changing the spacing between cavities influences the interaction mechanisms, which in turn affect boiling performance. These observations are in agreement with the pioneering work of Chekanov (1977), Calka and Judd (1985), Judd (1988), and Zhang and Shoji (2003), who reported that the distance between cavities and the bubble departure diameter are characteristic parameters that play a vital role in defining the regimes for the different interaction mechanisms involved in the boiling process. Furthermore, Chai et al. (2002) actually emphasized the definition of a characteristic length scale that can be correlated with the interaction mechanisms occurring in pool boiling and thus with the resulting heat transfer coefficients. Teodori et al. (2013) further speculated that surface micropatterns may help to alter the local fluid flow, thus affecting the various terms of the heat flux, as defined by Han and Griffith (1962). For these reasons, an accurate theoretical prediction of heat flux and/or heat transfer coefficients for pool boiling on micropatterned surfaces must account for all of these parameters.

1.1 Existing Models and Correlations

Several attempts have been made to predict pool-boiling heat flux and heat transfer coefficients. Two approaches are mainly followed: one is based on modeling the phenomena (e.g., Tien, 1962; Gerardi et al., 2009); the other is based on the development of empirical correlations (e.g., Vachon et al., 1968; Jabardo and Silva, 1991). Modeling of nucleate boiling is approached in different ways by various researchers. A well-known model is based on heat flux partitioning, which considers that pool-boiling heat flux is the result of three governing concurring mechanisms: (1) natural convection in the region of the surface not influenced by the bubbles; (2) evaporation occurring during the bubble-growing period (term related to the latent heat of evaporation), and (3) so-called quenching due to the inflow of cold fluid on the heating surface and subsequent thermal boundary layer reformation after bubble departure.

Heat flux partitioning was proposed by Han and Griffith (1962) and later by several authors, such as Gerardi et al. (2009). Although one must recognize that these models are based on partitioning of the heat flux in various terms—many of them strictly related to nucleation and bubble formation are quite representative of the physics governing the observed phenomena—the formulation expressing the different heat transfer mechanisms based on this approach is often strongly related to experimental data, such as bubble departure frequencies and diameters and nucleation site density, which are difficult to quantify accurately. Consequently, these models have a strong empirical nature and depend on the availability and accuracy of the existing experimental data. To contour this issue, several authors proposed modeling nucleate boiling via dimensional analysis, thus avoiding the use of quantities that must be obtained experimentally. Examples of this methodology are the correlations reported by Rohsenow (1952), Borishansky et al., (1961), Borishansky (1969), and Stephan and Abdelsalam (1980). Despite these efforts, after analyzing the existing correlations, it becomes clear that they are still strongly empirical because the fitting parameters are often derived and validated for particular experimental conditions. On the other hand, they are not adequate to describe pool-boiling on micropatterned surfaces given that, except for the Rohsenow correlation (1952), these correlations do not usually take into account the effect of either the surface/fluid combination or the surface microstructure. Some of them (including the Rohsenhow correlation) address the effect of surface topography by considering an average

surface roughness. However, this parameter is not representative of the geometric features of the surface pattern and so is weakly correlated with the quantities describing nucleation and bubble dynamics (McHale and Garimella, 2010).

The brief literature review just presented highlights the need to devise more tailored models and correlations, which include data obtained in experimental conditions similar to those reported for micropatterned surfaces with regular profiles (e.g., Nitesh et al., 2006; Moita et al., 2012; and Teodori et al., 2013). The regular micropatterns were characterized based on well-defined geometric quantities, which can actually be related to the nucleation process and to bubble dynamics. These relations are expected to be useful in deriving basic practical correlations that can later be included in more intricate computational models. Additionally, these semiempirical correlations can be used as engineering tools, guiding researchers toward a more systematic approach when deriving their surface micropatterns, because they should capture the basic physics governing the main processes involved in pool-boiling heat transfer on microstructured surfaces.

The current study investigated two approaches to devise a correlation for the specific case of pool boiling on microstructured surfaces with a regular pattern of cavities. The first approach consists of evaluating the performance of a Rohsenow-type correlation and then determining the fitting parameters as proposed by Vachon et al. (1968), Sauer et al. (1975), Jabardo and Silva (1991), Pioro (1999), and Jabardo et al. (2004). Based on this analysis, a modified Rohsenow correlation was proposed that still has the aforementioned empirical nature.

In the second approach, original correlations were devised based on dimensional analysis of the phenomena, which are strongly related to the effect of the surface topography. The independent data required for validation of the proposed relations were collected by coupling high-speed visualization and image postprocessing with heat flux/surface temperature measurements, following the methodology reported in Teodori et al. (2013).

2. EXPERIMENTAL APPROACH

2.1 Experimental Set-Up

The experimental data required for validation of the devised correlations were obtained as in Moita et al. (2012) and in Teodori et al. (2013) for the pool boiling of the dielectric fluid HFE 7000, ethanol, and water. The results reported by Nitesh et al. (2006) for the pool boiling of FC 72 are presented for comparative purposes given that the experimental conditions considered in Nitesh et al. are very similar to those addressed here. The relevant thermophysical properties of the working fluids are reported in Table 1. The experimental set-up, experimental procedure, and measurement uncertainties are only briefly described. A more detailed description can be found in Moita et al. (2012, 2015) and in Teodori et al. (2013).

The experimental arrangement comprised a power supply, a pool-boiling test section [Fig. 1(a)], a high-speed camera (Phantom v4.2 with 512 $\times$ 512 pixels @ 2,100 fps, and a maximum frame rate of 90 kfps; Vision Research, Wayne, NJ) and a DAQ acquisition system [Fig. 1(b)]. The temperatures were sampled using K-type thermocouples. The signal was acquired and amplified with a National Instruments DAQ board (National Instruments, Austin, TX) plus a BNC2120 (National Instruments, Austin, TX). The acquisition frequency was 100 Hz, and the temperature was

TABLE 1: Thermophysical properties of the fluids used in the present study (adapted from Nitesh et al., 2006; Moita et al., 2012; and Teodori et al., 2013)

	T_{sat} (°C)	ρ_l (kg/m^3)	ρ_v (kg/m^3)	μ_l (mN m/s^2)	c_{pl} [J/(kgK)]	k_l [W/(m.K)]	h_{fg} (kJ/kg)	σ_l (N/m) $\times$ 10^3
Water	100	957.8	0.5956	0.003	4217	0.68	2257	58
Ethanol	78.4	736.4	1.647	0.004	3185	0.165	849.9	17
FC 72	56	1,620.9	13.01	0.004	1,096	0.0583	84.73	9.5
HFE 7000	34	1,374.7	4.01	0.003	1,352.5	0.07	142	12.4

Note: The properties of FC 72 were adapted from Mudawar and Anderson 1990. T_{sat} = saturation temperature of the fluids; ρ = density; μ = dynamic viscosity; C_p = specific heat; k = thermal conductivity; h_{fg} = latent heat of evaporation; σ_l = liquid surface tension; l = liquid phase; and v = vapor phase.

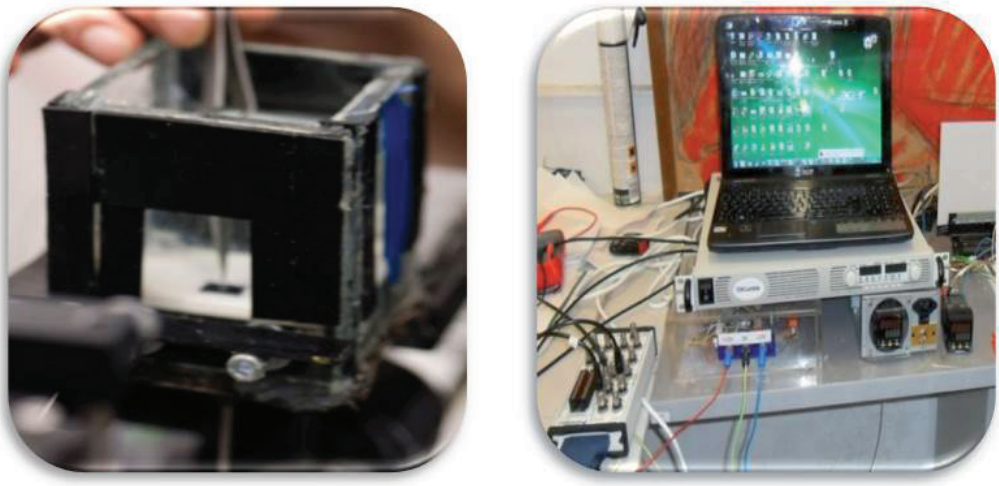

(a) (b)

FIG. 1: (a) Detail of the pool-boiling section; **(b)** DAQ system.

monitored for 20 seconds after reaching a stable condition (constant temperature variation not exceeding $\pm 0.5^{\circ}$C). The working fluid was preheated and degassed in a prechamber.

The heating section comprised a square aluminum support inside of which two cartridge heaters (125 W each) were inserted. The pool-boiling chamber was made of glass and sealed with rubber gaskets and high-temperature silicone. The dimensions of the tank were $60 \times 60 \times 70$ mm^3. Heaters attached to the sides of the pool-boiling chamber were controlled by a PID controller to ensure that the fluid remained in the chamber at the saturation temperature. The entire heating section of the pool-boiling test section was isolated with Teflon on the outside. This isolation allowed the heating power to be concentrated in the area of the silicon chip that was in contact with the aluminum support (1 cm^2). Two K-type thermocouples were placed at the center of the heating region, at z = 0 mm (in contact with the surface), z = 3 mm, and z = 5 mm.

2.2 Characterization of Surface Topography and Description of Wetting Behavior

The structured surfaces addressed here were the same used in Moita et al. (2012) and Teodori et al. (2013). They were custom-made from silicon wafers, which were first coated with aluminium (to allow a deeper etching) and then with photoresist. The regular patterns were transferred by high-resolution printing and photolithography and then submitted to plasma etching for 5–7 hours. Finally, wet etching was used to remove the aluminium coating. The microstructured surfaces resulting from this process had micropatterns of regular arrays of squared cavities with fixed length a = 52 μm and fixed depth h_R = 20 μm. The distance between the centers of the cavities, S, was the only variable distance, ranging 300 μm $< S <$ 1,200 μm. The parameters characterizing the micropatterns are shown schematically in Fig. 2(a), together with a photo of one of the surfaces [Fig. 2(b)]. Slight rounding of the edges of the cavities may have occurred, but their seemingly round shape in the figure is an optical distortion caused by the camera position.

The surfaces were characterized by their topography and wettability. The topography was evaluated from roughness profiles taken with a Dektak 3 profile meter with a vertical resolution of 200 angstroms (Veeco, Plainview, NY).

Wettability was quantified by the equilibrium contact angle, θ, using an optical tensiometer (Theta, Attension, Biolin Scientific, Stockholm, Sweden). The measurements were taken at room temperature (20°C) using the pendant drop method. The angles were evaluated from the images taken with the tensiometer using a camera coupled to a microscope. The images (resolution 15.6 μm/pixel for the optical configuration used here) were postprocessed

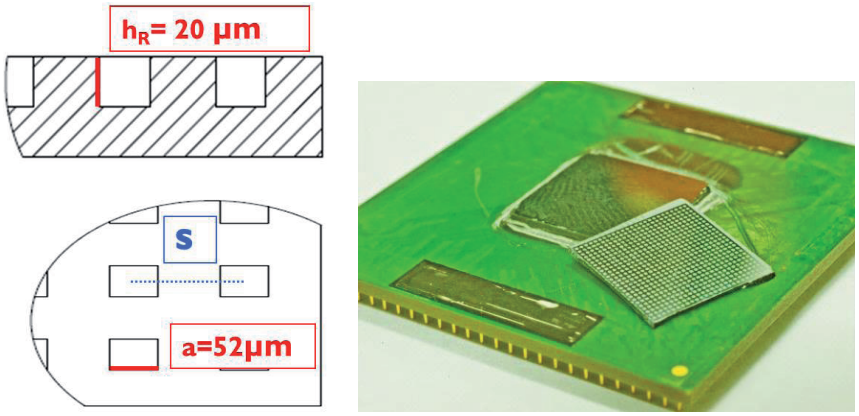

(a) (b)

FIG. 2: (a) Identification of the main parameters quantifying the micropatterns; **(b)** sample microstructured surface.

using a drop detection algorithm based on the Young-Laplace equation (Onte Attension software, Biolon Scientific, Stockholm, Sweden). The accuracy of drop detection algorithms is argued to be on the order of $\pm 0.1^\circ$ (Cheng, 1990). An averaged value of the equilibrium angle was obtained for each fluid/surface pair, derived from at least five measurements taken at different surface regions. Variations around the averaged value were observed to be between $\pm 1^\circ$ and $\pm 4^\circ$ and were attributed to hysteresis. Detailed measurement procedures are given in Moita et al. (2012).

Aging of the surfaces was periodically checked by repeating the characterization of the topography and by regularly measuring the contact angle. Any significant modifications were detected during the work reported here.

Table 2 summarizes the main topographical characteristics of the surfaces used in this study. It includes the average values of the equilibrium contact angles measured with water at room temperatures. The equilibrium angles obtained with ethanol and HFE 7000 in contact with all of the surfaces are close to zero. The table also summarizes the values of the true wetted area (liquid-solid contact area) of the microstructured surfaces, A_{en}.

Classical wetting theory mainly distinguishes homogeneous and heterogeneous wetting regimes. In a homogeneous wetting regime, the liquid completely wets the surface, thus penetrating the roughness grooves. The apparent contact angle measured at the rough surfaces in this regime is given by the contact angle resulting from the equilibrium of the interfacial tensions between the liquid, the solid, and the vapor interfaces (as defined by Young, 1805), corrected with the roughness factor r_f, which represents the ratio between the true and apparent wetted areas: $\theta_{\text{Wenzel}} = r_f \theta_{\text{Young}}$. This is the Wenzel equation (Wenzel, 1936). In the heterogeneous regime, described by the Cassie and

TABLE 2: Main range of micropatterned surface topographical characteristics

Material	**Reference**	a (µm)	h_R (µm)	S (µm)	θ (°)	A_{en}/A_{smooth} (-)
Silicon Wafer	Smooth	≈ 0	≈ 0	≈ 0	86.0	1
	C1	52	20	304	90.0	1.0675
	C2	52	20	400	91.5	1.0392
	C3	52	20	464	71.5	1.0275
	C4	52	20	626	86.5	1.0159
	C5	52	20	700	95.0	1.0122
	C6	52	20	800	60.5	1.0089
	C7	52	20	1,200	66.3	1.0039

Note: θ is the average static contact angle measured with water at room temperature; $\theta \cong 0^\circ$ for all surfaces in contact with ethanol and HFE 7000.

Baxter equation (Cassie and Baxter, 1944), the liquid does not completely penetrate the rough grooves.

Despite the relatively simple approach used, establishing accurate wetting regimes for a certain condition is still a topic of discussion because the sensitivity of the macroscopic apparent angle to the actual topographical characteristics of the surface depends on the relative size and scale being considered (e.g., Gao and McCarthy, 2007; Marmur, 2011; Moreira, 2014; Cheng et al., 2014). Following the Wenzel equation, one should expect the contact angle to increase with A_{en}. However, as reported in the aforementioned and other studies, although the Wenzel equation provides macroscopically good approximations to estimate the contact angle in the homogeneous wetting regime (which was identified to occur in the current study), it does not address the phenomena occurring at the contact line. Moreover, experimental results do not always confirm this trend of the contact angle (e.g., Kandlikar and Steinke, 2001). In the current study, as far as one could observe from visual inspection (using the microscope of the tensiometer), the liquid wetted the surface in a regime close to that described by Wenzel, but the microscopic roughness of the silicon wafers was very small and so the apparent contact angle was not sensitive to it. After etching, this microscale stochastic roughness was observed to increase. This increase was not quantified, although, from the roughness profiles, it could be estimated to be on the order of 0.5 μm, which is high enough to increase the contact angle, as reported by Moita and Moreira (2003). As the number of cavities increases (i.e. as A_{en} increases and S decreases), the microroughness is more likely to increase, although any trend can be devised because of the stochastic nature of the process. Given that A_{en} and S are determined solely based on the main dimensions of the micropatterns, they do not take this microroughness into account, so there is no linear relation between A_{en} (or S) and the apparent contact angle. The general trend that could be identified—a slight increase in θ from the surfaces with the lowest values of A_{en} (on the order of 60°, as observed for surfaces C6 and C7) to those with higher values of A_{en} (70–95° for all other surfaces)—was therefore speculatively attributed to the most probable formation of this microroughness during the etching process and not to a linear relation with the increase in A_{en}. A linear relation between the apparent contact angle and the roughness ratio, determined from the micrometric regular patterns, requires the fulfillment of particular relations between the depth of the cavities and the distance between them. An exhaustive review of this subject is beyond the scope of the present work, but an appropriate relation to differentiate between homogeneous and heterogeneous wetting can be derived based on the work of Jung and Bhushan (2008). Here, the governing geometric parameter is the ratio h_R/S, where h_R is the height/depth of the pillars/cavities and S is the distance between them. Following these researchers, a significant modification of the wetting regime, noticeable from the increase in the apparent contact angle, was observed only for values of $h_R/S > 0.25$. Thus, for the surfaces used here, $0.017 < h_R/S < 0.07$, which was expected to fall within an "apparent angle homogeneous wetting regime." The apparent contact angle had a very low sensitivity to this range of variation of h_R/S.

2.3 Experimental Procedure and Measurement Uncertainties

The boiling curves were determined for each fluid and each heating surface by varying the imposed heat flux in discrete steps (1–5 W). Temperature measurements were taken for each heat flux step when the system was considered to have attained equilibrium (i.e., when the temperature value oscillated around ±0.5°C). Individual curves were obtained from the average of four experiments. They were obtained by both increasing and decreasing the heat flux to account for hysteresis effects.

The main uncertainties of the quantities related to the heat transfer measurements are summarized in Table 3. The uncertainty in temperature measurements was assessed as recommended by Abernethy et al. (1985). A more comprehensive description of both the experimental procedures and the measurement uncertainties is provided in Moita et al. (2015).

3. RESULTS AND DISCUSSION

Pool-boiling curves were experimentally obtained for the three working fluids on the various microstructured surfaces (see Table 2). The results, reported in Fig. 3, highlight that water is generally characterized by higher heat transfer coefficient values because of the higher values of its thermophysical properties. The figure also shows that surface topography dramatically influences the heat transfer process. Therefore, decreasing the distance between cavities,

TABLE 3: Main uncertainties in quantities related to the heat transfer measurements

Measured parameter	Maximum combined uncertainty	Evaluation method
Heat flux, $q^{"}$ (W/cm^2)	$\pm$22.5% (fully developed nucleate HFE 7000 boiling)	$\Delta q^{"}/q^{"} = \left[(\Delta L/e)^2 + (\Delta T/T)^2\right]^{1/2}$ e = thickness of heating surface for which heat flux evaluated
Temperature, T (°C)	$\pm$1.2°C	$unc_T = \left[B^2 + t_{95} STD^2\right]^{1/2}$ B = bias limit, t_{95} = confidence level; STD = standard deviation
Heat transfer coefficient, h (W/cm^{2}K)	$\pm$22.5% (fully developed nucleate HFE 7000 boiling)	$\Delta h/h = \left[\left(\Delta q^{"}/q^{"}\right)^2 + (\Delta T/T)^2\right]^{1/2}$

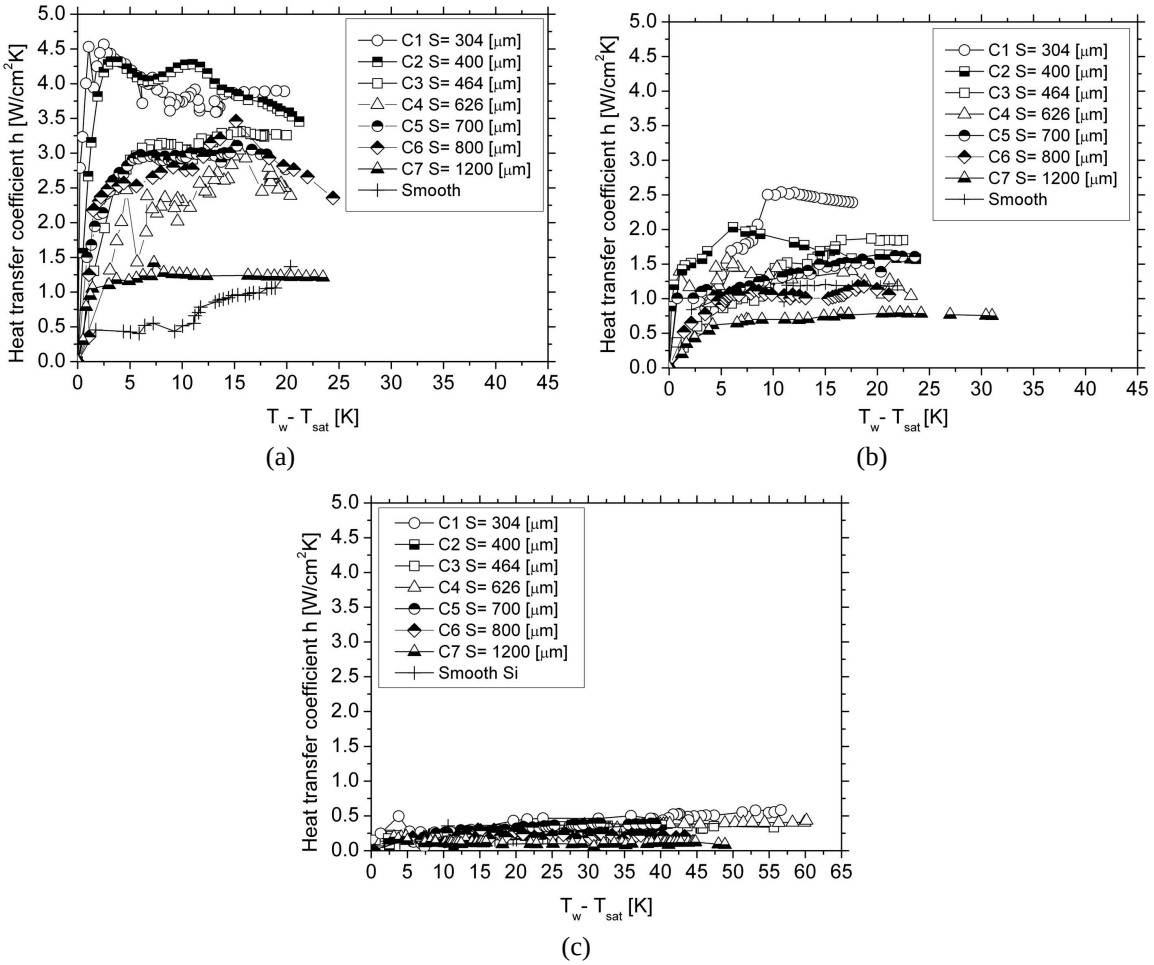

FIG. 3: Heat transfer coefficient versus wall superheat for the fluids studied, boiling on microstructured surfaces: **(a)** water, **(b)** ethanol, and **(c)** HFE 7000.

thus increasing the number of cavities, leads to an increase in the heat transfer coefficients because of the increase in the true wetted area. Also, the larger number of cavities promotes a higher number of active nucleation sites. This is a straightforward trend for fluids with low surface tension such as HFE 7000 and ethanol. On the other hand, for fluids with higher surface tension, such as water, the larger bubbles that slowly depart from the surface (because of the higher surface tension and latent heat of evaporation) endorse the occurrence of strong horizontal coalescence, which for surfaces with a large number of cavities may actually lead to deterioration of the heat transfer coefficient, as reported by Nitesh et al. (2006) and Moita and Moreira (2012).

A practical representation of the combined effects of surface topography and fluid properties on pool-boiling heat transfer is shown in Fig. 4, which depicts the ratio between the averaged heat transfer coefficients obtained on the microstructured surfaces and that achieved on the smooth surface (h_{av}/h_{smooth}) as a function of the distance parameter, S/L_c. The ratio (h_{av}/h_{smooth}) expresses the relative enhancement in terms of heat transfer coefficients obtained by microstructuring the surface whereas S/L_c represents the ratio between the distance between the cavities and a parameter, L_c, which mainly represents the capillary length and is indicative of the bubble departure diameter:

$$L_c = \sqrt{\frac{\sigma_l}{g \cdot (\rho_l - \rho_v)}} \tag{1}$$

The distance parameter S/L_c has been widely used (e.g., Chekanov, 1977; Calka and Judd, 1985; Judd, 1988; and Zhang and Shoji, 2003) to define different regions of interaction between cavities. Thus, it is adopted here to address the combined effects of the fluid/surface used because these combined effects are observed to mostly affect the interaction (e.g., coalescence) mechanisms.

Figure 4 also shows that, for low-wetting fluids such as water, decreasing S/L_c is only advantageous until a minimum value of S (which corresponds to surface C1, S = 304 μm in the present study). If S is further decreased, the negative effects of bubble interaction become dominant, leading to a deterioration of the heat transfer coefficient so that h_{av}/h_{smooth} decreases. This behavior contrasts with that observed in fluid boiling with lower surface tension, in which the interaction mechanisms play a secondary role (e.g., Moita et al., 2012; Teodori et al., 2013).

3.1 Development of Correlation—First Approach: Modified Rohsenow Correlation

According to Rohsenow (1952), heat transfer enhancement under boiling conditions is the result of local fluid circulation in the region close to the heating surface, promoted by successive bubble detachments. After some mathematical manipulation, the Rohsenow correlation can be rewritten as

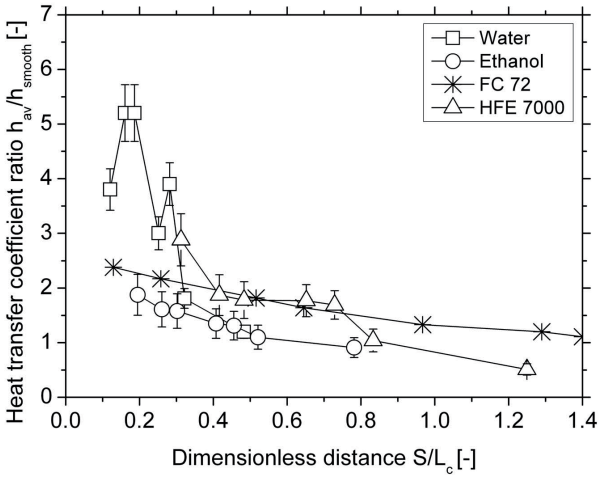

FIG. 4: Heat transfer ratio versus dimensionless distance for water, ethanol, and HFE 7000 in the range of patterns studied.

$$\frac{Cp_l \cdot \Delta T}{h_{fg}} = C_{sf}\left[\frac{q''}{\mu_l h_{fg}} \cdot \sqrt{\frac{\sigma_l}{g \cdot (\rho_l - \rho_v)}}\right]^m \cdot \mathrm{Pr}_l^n \tag{2}$$

or

$$\mathrm{St}^* = C_{sf} \cdot \mathrm{Re}_b^m \cdot \mathrm{Pr}_l^n \tag{3}$$

The lefthand side of the equation corresponds to the inverse of the Stanton number, St*, whereas the first term on the righthand side is the Reynolds number, referred to as the bubble departure diameter, Re_b, multiplied by the Prandtl number Pr = $\mu_l Cp_l/k_l$. Re_b, as introduced in the original Rohsenow correlation, is given by

$$\mathrm{Re}_b = \frac{V \cdot L_c}{\nu} = \frac{\rho_l \cdot V \cdot L_c}{\mu_l} \tag{4}$$

in which L_c is the characteristic length, as defined in Eq. (1) and

$$V\left[\frac{m}{s}\right] \propto \frac{L_c}{t_b} \propto \frac{L_c}{\left(\frac{\rho_l h_{fg} L_c^3}{q'' L_c^2}\right)} \propto \frac{q''}{\rho_l h_{fg}} \tag{5}$$

is a characteristic velocity that quantifies the stirring effect of the departing bubble in the surrounding liquid. The value t_b is the characteristic time between the departure of consecutive bubbles and can be estimated as the ratio between the energy required to form a vapor bubble, $\rho_l h_{fg} L_c^3$ and the rate at which heat is added to the solid-vapor contact area, $q'' L_c^2$.

Combining Eqs. (4) and (5), Re_b can be expressed as

$$\mathrm{Re}_b = \frac{\rho_l \cdot V \cdot L_c}{\mu} = \frac{\rho_l}{\mu} \cdot \sqrt{\frac{\sigma_l}{g \cdot (\rho_l - \rho_v)}} \cdot \frac{q''}{\rho_l h_{fg}} = \frac{q''}{\mu_l h_{fg}} \cdot \sqrt{\frac{\sigma_l}{g \cdot (\rho_l - \rho_v)}} \tag{6}$$

From this final equation it is clear that Re_b depends on the operating conditions established by the imposed heat flux and by the thermophysical properties of the fluid. Thus, for the conditions addressed in the current study, $0.3944 \leq \mathrm{Re}_b \leq 4.3791$ which corresponds to $-0.9302 \leq \ln \mathrm{Re}_b \leq 1.4768$. The distribution of Re_b is quite wide, as expected given the broad range of imposed heat flux values and the wide range of thermophysical properties of the fluids and the surfaces.

Rohsenow fitted the values of m and n to be equal to 0.33 and 1.7, or to 1.0 for water. According to Rohsenow, although m is not affected by surface properties, n may depend on surface finishing, so it can vary between 0.8 and 2.0. The numerical coefficient, C_{sf}, is related to the effect of the fluid/surface combination by means of the equilibrium contact angle, θ. This fitting parameter, C_{sf}, is argued to also include the effect of surface roughness, but any explicit relation is proposed.

It is worth mentioning that the Rohsenow correlation has been validated only for experimental data corresponding to a fully developed nucleate boiling regime, considering that all cavities act as active nucleation sites.

3.1.1 First Fitting—Rohsenow n (1–1.7) and m (0.33): C_{sf} Evaluated

The fitting procedures reported here are similar to those proposed by Jabardo et al. (2004). Detailed derivations of the formulas are described in the Appendix. The first fitting process is maintaining the original exponents of the Rohsenow equation and determining C_{sf} for the different surface/fluid combinations. The method used was the linearization of the equation by expressing it in terms of logarithms and then processing the data through regression analysis. Hence, Eq. (3) in logarithmic terms becomes

$$\ln \mathrm{St}^* = a1 + m \cdot \ln \mathrm{Re}_b + n \cdot \ln \mathrm{Pr} \tag{7}$$

where $a1 = \log C_{sf}$.

For the surfaces used here, the main role of the microstructure was captured by the distance between cavities, S, which is associated with the interaction mechanisms, and by the increased wetted area A_{en}/A_{smooth}. Both parameters were taken into account in a new geometric parameter, proposed in the form: $[(L_c/S) \cdot (A_{en}/A_{smooth})]$. By doing so, the first fitting procedure shows that the values of C_{sf} obtained during this fitting procedure are strongly dependent on the surface topography. This trend, which is clearly depicted in Fig. 5, is in agreement with the results reported by Jabardo et al. (2004): the values of C_{sf} decrease when the geometry parameter increases.

The results, presented in Fig. 5, were fitted by a correlation with the following general form (Teodori et al., 2014):

$$C_{sf} = a \cdot \ln\left(\frac{L_c}{S} \cdot \frac{A_{en}}{A_{smooth}}\right) + b \tag{8}$$

The coefficients a and b vary with the different fluids, as reported in Table 4. The general form of Eq. (8) was derived after exhaustive search of numerous possible functions (linear, exponential, and logarithmic) to find the one providing the best fit to the experimental data, following the trend discussed previously. A similar procedure was adopted by Jabardo et al. (2004), although they tried to correlate C_{sf} with the average roughness, R_a.

The fitting constants were determined using the least-squares method. A more detailed explanation of the derivation of this expression and the determination of the fitting constants is given in the Appendix.

In Table 4, "max (Res)" indicates the maximum value of the residuals and "Res_norm" indicates the sum of squares of the residuals. The evaluation of this first fitting procedure is depicted in Fig. 6. Most of the data fall within the range of $\pm 20\%$, indicated by the two straight continuous lines. Furthermore, the agreement between the correlation and the experimental data from Nitesh et al. (2006) is rather good. These positive results endorsed an attempt to perform a more general fitting, with the aim of obtaining a more universal relation.

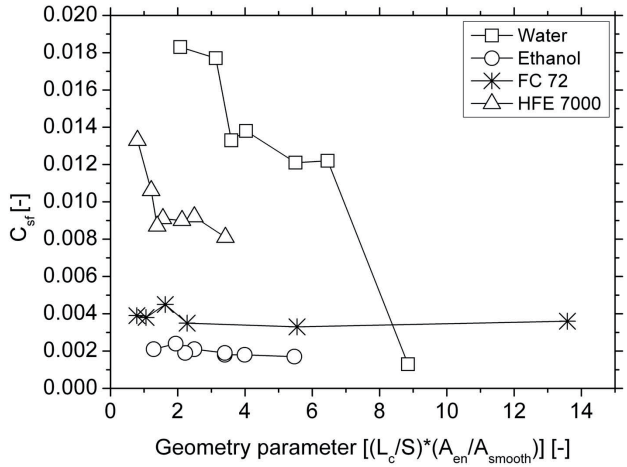

FIG. 5: Evaluated values of C_{sf} versus the geometric parameter $[(L_c/S) \cdot (A_{en}/A_{smooth})]$ for water, ethanol, and HFE 7000 (current study), and for FC 72 (Teodori et al., 2014).

TABLE 4: Fitting coefficient for the relationship between C_{sf} and $[(L_c/S) \cdot (A_{en}/A_{smooth})]$

	HFE 7000	**FC 72**	**Ethanol**	**Water**
a	-0.0033	-0.0007	-0.0007	-0.0059
b	0.0115	0.0047	0.0028	0.0200
max (Res)	0.000749	0.000293	0.000145	0.000938
Res_norm	0.000054	0.000037	0.000054	0.000094
R^2	0.9254	0.9708	0.9825	0.9574

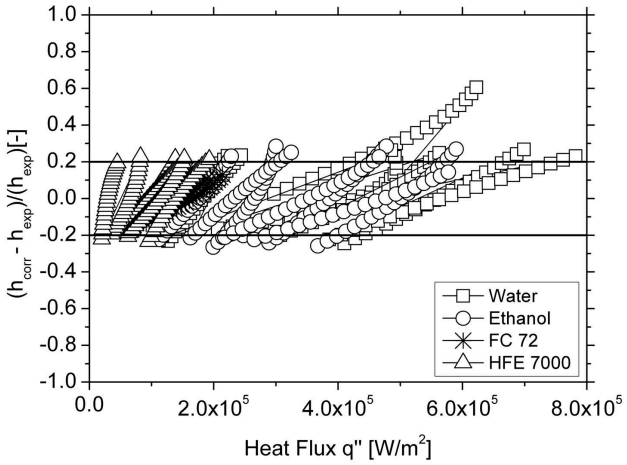

FIG. 6: Evaluation of the first fitting process for water, ethanol, and HFE 7000 (current study), and for FC 72 (Teodori et al., 2014).

3.1.2 Second Fitting (n, m, and C_{sf} Evaluated)

Assessment of m The experimental data obtained for the different fluids were represented in plots ln St* versus ln Re$_b$. The values of m for each fluid/surface combination were determined by

$$\ln \mathrm{St}^* = m \cdot \mathrm{Re}_b + C \tag{9}$$

The m values were found to be dependent on the fluid and from the surface properties, as shown in Fig. 7. A closer analysis of this figure allows identification of a common general slope for all surface/fluid combinations studied here. This trend was also in agreement with the analysis performed by Jabardo et al. (2004).

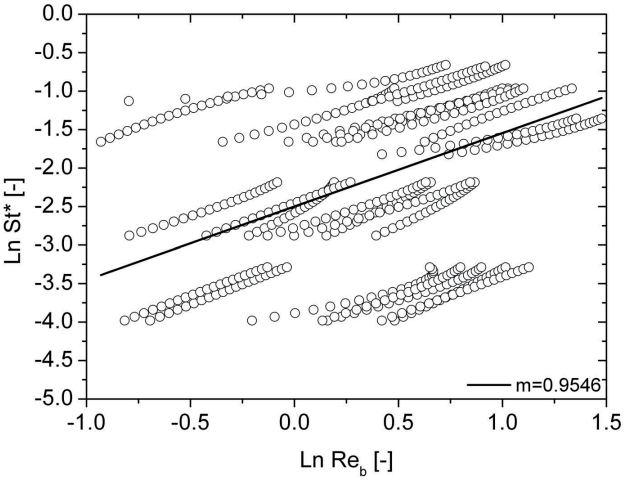

FIG. 7: Determination of m for the Rohsenow correlation for water, ethanol, and HFE 7000 (current study), and for FC 72 (Teodori et al., 2014).

Assessment of C_{sf}, n The remaining fitting constants of the Rohsenow equation were assessed based on the following assumptions:

- C_{sf} is a function of the geometric parameter $[(L_c/S) \cdot (A_{en}/A_{smooth})]$, in agreement with the first fitting procedure.
- The value of n does not depend on the pressure, but, like C_{sf}, is a function of $[(L_c/S) \cdot (A_{en}/A_{smooth})]$. Although not entirely proven, this hypothesis was also raised by Vachon et al. (1968), who argued that n can indeed be affected by the properties of the surface/fluid combinations. Jabardo et al. (2004) also considered this possibility.

Following these assumptions, the Rohsenow correlation assumes a new form, in which surface topography plays a dominant role. The final correlation in the logarithm form is here proposed as:

$$\ln \mathrm{St}^* - m \cdot \ln \mathrm{Re}_b = a1 \cdot \ln \left[\frac{L_c}{S} \cdot \frac{A_{en}}{A_{smooth}} \right] + a2 \cdot \left[\frac{L_c}{S} \cdot \frac{A_{en}}{A_{smooth}} \right] \cdot \ln \mathrm{Pr} + C \tag{10}$$

The parameters $a1$ and $a2$, and the constant C, which were found through regression analysis, are summarized in Table 5. A more comprehensive derivation of this equation and of the respective fitting parameters is provided in the Appendix.

The resulting heat transfer coefficients, evaluated based on this new correlation, are depicted in Fig. 8. With most of the data falling within the range $\pm 20\%$, this modified Rohsenow correlation also seems to be suitable for prediction purposes. Furthermore, it is in fairly good agreement with the experimental data reported by Nitesh et al. (2006).

TABLE 5: Fitting coefficient for the modified Rohsenow correlation

	HFE 7000	**FC 72**	**Ethanol**	**Water**
C	0.1177	0.2187	0.1379	0.0521
$a1$	−2.7068	−1.1551	−0.9879	−1.3696
$a2$	0.5144	0.0606	0.0384	0.2454
max (Res)	0.0363	0.0666	0.0098	0.0066
Res_norm	0.0455	0.3457	0.0034	0.0036
R^2	0.9885	0.8699	0.9811	0.9049

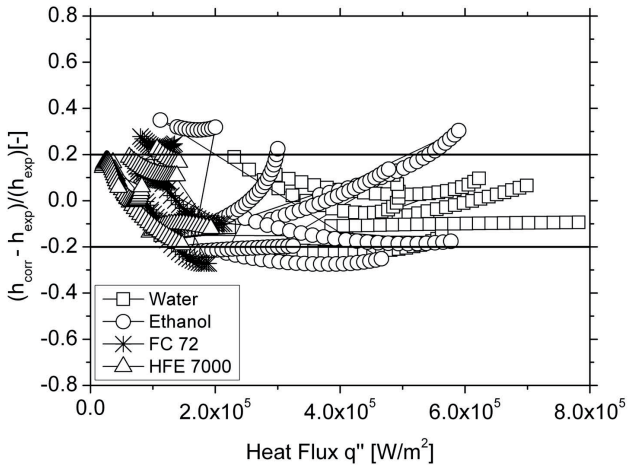

FIG. 8: Evaluation of the modified Rohsenow correlation for water, ethanol, and HFE 7000 (current study), and for FC 72 (Teodori et al., 2014).

The procedure proposed up to now was a first attempt to include the combined effect of the distance between cavities and the enhancement of the true wetted area of the microstructured surfaces in correlations predicting the pool-boiling heat transfer coefficients by introducing a new geometric parameter. Despite being reasonably successful, this approach still required continuous adjustment of the fitting parameters, thus losing generality. In this context, new correlations are proposed, based on a dimensional analysis, as described in the following paragraphs.

3.2 Development of Correlations—Second Approach: Dimensional Analysis

The proposed correlations were based on the Buckingham (pi) theorem to formulate the independent variables chosen to represent the dependent parameter. According to the Buckingham (pi) theorem, a given set of $q_1, q_2, q_3, \ldots, q_n$, n-dimensional variables, which are physically relevant to a given problem and interrelated by an (unknown) dimensionally homogeneous set of equations, can be expressed by a functional relationship in the form

$$F\left(q_1, q_2, q_3, \ldots, q_n\right) = 0 \quad \text{or} \quad q_1 = f\left(q_2, \ldots, q_n\right) \tag{11}$$

If k is the number of fundamental dimensions required to describe the n variables, then there are k primary variables and the remaining j = $(n - k)$ variables can be expressed as $(n - k)$ dimensionless and independent quantities of pi groups $\Pi_1, \Pi_2, \ldots, \Pi_{n-k}$. Hence, the functional relationship can be reduced to the much more compact form

$$\Phi\left(\Pi_1, \Pi_2 \ldots \Pi_{n-k}\right) = 0 \quad \text{or} \quad \Pi_1 = \Phi\left(\Pi_2, \ldots, \Pi_{n-k}\right) \tag{12}$$

To define the n variables that characterize the problem, it was assumed that the pool-boiling heat transfer can be related to

- The thermophysical properties of the fluid—namely, latent heat of evaporation, thermal conductivity, specific heat, and saturation temperature.
- The variable related to the operating conditions being imposed heat flux.
- The influence of the surface properties being captured by the combined effect of the distance between cavities and the enhancement of the true wetted area of the microstructured surfaces. These parameters were included in the new geometric parameter $[(L_c/S) \cdot (A_{en}/A_{smooth})]$, which, according to the discussion in the previous paragraphs, plays a determinant role in pool-boiling heat transfer.
- It being widely accepted that the characteristic dimension, L_c, as defined in Eq. (1) is representative of the bubble departure diameter and the thickness of the thermal boundary layer.

Following this reasoning, eight variables were selected ($hq^{''} L_c (L_c/S) \cdot (A_{en}/A_{smooth})$, $k_l T_{sat} Cp_l$, h_{fg}), which are related to four fundamental dimensions $\{MLT\theta\}$. Consequently, four pi groups were defined. In the assessment of the required criteria for pi grouping, the considerations discussed in the following paragraphs were taken into account:

The pool-boiling heat transfer coefficient is widely expressed in terms of the Nusselt number, which represents the ratio between the heat transferred by convection and that transferred by conduction. Thus, the Nusselt numberm defined as

$$\frac{h \cdot L_c}{k_l} \tag{13}$$

is the first pi group. The second pi group is the geometric parameter

$$\frac{L_c}{S} \cdot \frac{A_{en}}{A_{smooth}} \tag{14}$$

However, as briefly discussed in the Introduction, heat flux can be divided into three governing concurring mechanisms: natural convection, evaporation occurring during the bubble-growing period (term associated with latent heat),

and quenching due to the inflow of cold fluid on the heating surface and subsequent thermal boundary layer reformation after bubble departure. Quenching has been experimentally observed by others to play a dominant role in the region of the pool-boiling curve addressed in the current study (e.g., Gerardi et al., 2009; Teodori et al., 2013). Hence, the third pi group attempts to account for the percentage of heat removed by this mechanism and is proposed to be given by

$$\frac{q'' \cdot L_c}{k_l \cdot T_{sat}} \tag{15}$$

In Eq. (15), T_{sat} was chosen instead of ΔT_{sat} because, although superheat is more relevant in terms of heat transfer analysis, it depends on measured quantities whereas T_{sat} is a characteristic property of the working fluid. From the perspective of the formulation, parameters related only to the thermophysical properties of the working fluids were the preferred choice. Furthermore, using ΔT_{sat} would have added a parameter that depends on the operating conditions, thus influencing the fitting procedure.

The last pi group was devised based on the modified Stanton number:

$$\frac{h_{fg}}{Cp_l \cdot T_{sat}} \tag{16}$$

With all pi groups identified, the new correlation proposed here for pool-boiling heat transfer can be rearranged in the form

$$\frac{h \cdot L_c}{k_l} = C \cdot \left[\frac{L_c}{S} \cdot \frac{A_{en}}{A_{smooth}}\right]^{a1} \cdot \left[\frac{q'' \cdot L_c}{k_l \cdot T_{sat}}\right]^{a2} \cdot \left[\frac{h_{fg}}{Cp_l \cdot T_{sat}}\right]^{a3} \tag{17}$$

After regression analysis, the final formulation is given by

$$\frac{h \cdot L_c}{k_l} = 24.1051 \cdot \left[\frac{L_c}{S} \cdot \frac{A_{en}}{A_{smooth}}\right]^{0.2822} \cdot \left[\frac{q'' \cdot L_c}{k_l \cdot T_{sat}}\right]^{0.6661} \cdot \left[\frac{h_{fg}}{Cp_l \cdot T_{sat}}\right]^{0.1884} \tag{18}$$

A more detailed description of the formulation and determination of the fitting parameters for Eq. (18) is provided in the Appendix.

Figure 9 depicts the heat transfer coefficients evaluated with this correlation. Most of the data are in good agreement with the relation, within an error of $\pm 30\%$. Such good agreement is indicative of the derived correlation's consistent ability to capture the governing processes given that the experimental data depicted in the figure were obtained

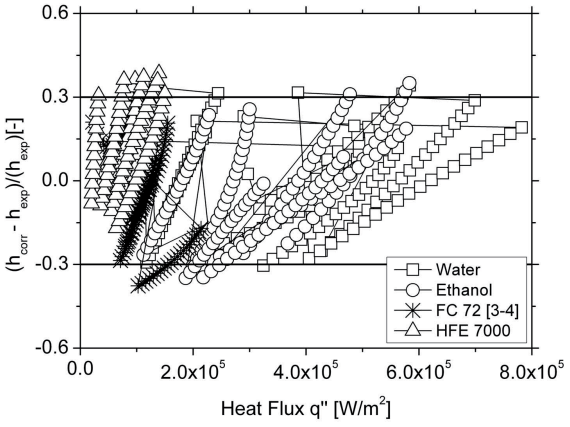

FIG. 9: Evaluation of the first dimension-based correlation for water, ethanol, and HFE 7000 (current study), and for FC 72 (Teodori et al., 2014).

using 30 different surface fluid/combinations and included results reported in the literature. Furthermore, the various fluids tested here have significantly different thermophysical properties, which were well captured by the correlation. From these encouraging results, one can infer that the dimensional analysis performed here is indeed a suitable way to determine a more general correlation, which can be used for a wider range of pool-boiling configurations.

3.2.1 New Correlation Based on The Heat Flux Partitioning Model

Following the procedure described in previous paragraphs, the following approach considers the use of all terms associated with heat flux partitioning to devise a new correlation instead of considering just the term related to quenching. From the variables chosen to characterize the problem ($hq^{''}L_c(L_c/S)\cdot(A_{en}/A_{smooth})$, $k_l T_{sat} Cp_l$, $h_{fg}\rho_v$), five pi groups had to be defined. The Nusselt number, the geometric parameter, and the pi group associated with quenching, as defined in Eqs. (13)–(15) were readily identified. The term related to the percentage of heat removed by evaporation (i.e., associated with the latent heat of evaporation) is proposed as

$$\frac{q^{''}}{h_{fg}^{1,5}\rho_v} \tag{19}$$

The last pi group accounts for the relation between the dynamic phenomena involved in the pool-boiling process and the quenching heat flux term:

$$\frac{q^{''}\cdot L_c\cdot Cp_l}{k_l\cdot h_{fg}} \tag{20}$$

To understand the meaning of this last group, one can slightly modify the expression in the following way:

$$\frac{q^{''}\cdot L_c\cdot Cp_l\cdot T_{sat}}{k_l\cdot T_{sat}\cdot h_{fg}} \tag{21}$$

where the terms related to the heat removed by quenching and to the modified Stanton number are readily identified. This last group accounts for the important role of bubble dynamics in the pool-boiling heat transfer process (e.g., Teodori et al., 2013). It should be mentioned that these pi groups were not deduced. Instead, a home-made routine was devised in MATLAB, which allowed combining the chosen variables following the Buckingham theorem. Once the variables were selected and the fundamental dimensions were reported in the code, the pi groups were unequivocally defined.

It is worth mentioning that in this last dimensional analysis all pi groups were related to heat flux, which is actually a violation of the Buckingham theorem because the dimensionless groups should be independent. However, the aim of the correlation depicted here was to emphasize the relative importance of the various terms of the heat flux.

The final correlation can be expressed in the form

$$\frac{h\cdot L_c}{k_l} = C\cdot\left(\frac{L_c}{S}\cdot\frac{A_{en}}{A_{smooth}}\right)^{a1}\cdot\left(\frac{q^{''}\cdot L_c}{k_l\cdot T_{sat}}\right)^{a2}\cdot\left(\frac{q^{''}}{h_{fg}^{1,5}\rho_v}\right)^{a3}\cdot\left(\frac{q^{''}\cdot L_c\cdot Cp_l}{k_l\cdot h_{fg}}\right)^{a4} \tag{22}$$

After regression analysis, the final formulation becomes

$$\frac{h\cdot L_c}{k_l} = 12359\cdot\left(\frac{L_c}{S}\cdot\frac{A_{en}}{A_{smooth}}\right)^{0.3366}\cdot\left(\frac{q^{''}\cdot L_c}{k_l\cdot T_{sat}}\right)^{0.8675}\cdot\left(\frac{q^{''}}{h_{fg}^{1,5}\rho_v}\right)^{-0.3715}\cdot\left(\frac{q^{''}\cdot L_c\cdot Cp_l}{k_l\cdot h_{fg}}\right)^{-0.0453} \tag{23}$$

(see the Appendix for more details). As shown in Fig. 10, most of the data are in good agreement with the relation, within an error of $\pm$30%, which is similar to the correlation proposed in the previous subsection. Based on this good agreement, one may argue that the quenching term proposed in the previous correlation in fact plays the dominant role, as suggested by Gerardi et al. (2009), so that including the other terms in the correlation may actually be redundant and may not improve the relation.

Nevertheless, the last proposed correlation also accounts for the heat flux related to vaporization and thus describes more accurately the phenomena involved in the boiling process. This term was observed to decrease as the heat flux increased, which is in agreement with observations reported in Gerardi et al. (2009).

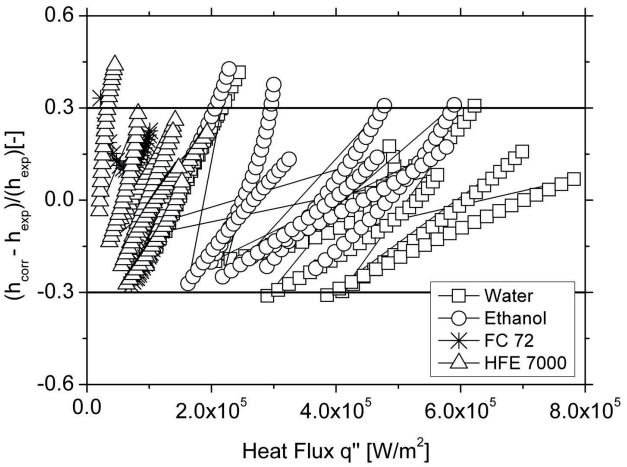

FIG. 10: Evaluation of the second dimension-based correlation for water, ethanol, and HFE 7000 (current study), and for FC 72 (Teodori et al., 2014).

4. CONCLUSIONS

The present paper proposes correlations to predict the heat transfer coefficient for pool boiling of various fluids on micropatterned silicon wafer surfaces, following two approaches. The first consisted of determining a modified Rohsenow correlation, with emphasis given to the introduction of a new geometric parameter that can accurately describe the topology of the surfaces used in the experiments. The correlation devised can predict the pool-boiling heat transfer coefficient for various fluid/surface combinations, including additional data reported in the literature, within an error of $\pm 20\%$. In a second approach, original relations were devised based on dimensional analysis.

ACKNOWLEDGMENTS

The authors are grateful to Fundação para a Ciência e a Tecnologia (FCT) for partially funding this research in the framework of projects PTDC/EME-MFE/109933/2009 and RECI/EMS-SIS/0147/2012. The authors also acknowledge FCT for supporting E. Teodori with a Ph.D. fellowship (Ref. :SFRH/BD/88102/2012) and A. S. Moita with a postdoctoral fellowship (Ref. :SFRH/BPD/63788/2009).

REFERENCES

Abernethy, R. B., Benedict, R. P., and Dowdell, R. B., ASME measurement uncertainty, *J. Fluids. Eng.*, vol. **107**, no. 2, pp. 161–164, 1985.

Anderson, T. M. and Mudawar, I., Microelectronic cooling by enhanced pool boiling of a dielectric fluorocarbon liquid, *ASME J. Heat Transf.*, vol. **111**, pp. 752–759, 1989.

Borishansky, V. M., Correlation of the effect of pressure on critical heat flux and heat transfer rates using theory of thermodynamic similarity, In: *Problems of Heat Transfer and Hydraulics of Two-Phase Media*, New York: Pergamon Press, pp. 16–37, 1969.

Borishansky, V. M., Bodrovich, B. I., and Minchenko, F. P., Heat transfer during nucleate boiling of water and ethyl alcohol, In: Kutateladze, S. S., ed., Aspects of heat transfer and hydraulics of two-phase mixtures, Moscow, Govt. Energy Publishing House, pp. 75–93, 1961.

Calka, A. and Judd, R. L., Some aspects of the interaction among nucleation sites during saturated nucleate boiling, *Int. J. Heat Mass Transf.*, vol. **28**, pp. 2331–2342, 1985.

Cassie, A. B. and Baxter, S., Wettability of porous surfaces, *Trans. Faraday Soc.*, vol. **40**, pp. 546–551, 1944.

Chai, L. H., Shoji, M., and Peng, X., Bubble interaction in thermal boundary layers, *Tsinghua Sci. Tech.*, vol. **7**, no. 17, pp. 160–164, 2002.

Chekanov, V. V., Interaction of centers in nucleate boiling, *Teplofiz. Vys. Temp.*, vol. **15**, pp. 121–128, 1977.

Cheng, P., Automation of axisymmetric drop shape analysis using digital image processing [dissertation], Toronto: University of Toronto, 1990.

Cheng, P., Quan, X. J., Gong, S., and Hong, F. J., Recent studies on surface roughness and wettability effects in pool boiling, *Proc. of the* 14^{th} *IHT*, Kyoto, Japan, August 10–15, 2014.

Gao, L. and McCarthy, T. J., How Wenzel and Cassie were wrong, *Langmuir*, vol. **23**, no. 7, pp. 3762–3765, 2007.

Gerardi, C., Buongiorno, J., Hu, L. W., and McKrell, T., Measurement of nucleation site density, bubble departure diameter and frequency in pool boiling of water using high-speed infrared and optical cameras, *Proc. of the 7th ECI International Conference on Boiling Heat Transfer*, Florianopolis, Brazil, May 3–7, 2009.

Han, C. Y. and Griffith, P., The mechanism of heat transfer in nucleate boiling, Technical Report No. 7673-19, Department of Mechanical Engineering, Massachusetts Institute of Technology, 1962.

Honda, H., Takamatsu, H., and Wei, J. J., Enhanced boiling of FC-72 on silicon chips with micro-pin-fins and submicro-scale roughness, *ASME J. Heat Transf.*, vol. **124**, pp. 383–390, 2002.

Jabardo, J. M. S. and Silva, C. L., Modeling of the nucleate boiling of refrigerant-oil mixtures, *Proc. of the 18th Intl. Congress of Refrigeration*, Montreal, August 10–17, 1991.

Jabardo, J. M. S., Silva, E. F., and Barros, S. F., Evaluation of the Rohsenow correlation through experimental pool boiling of halocarbon refrigerants on cylindrical surfaces, *J. Braz. Soc. Mech. Sci. & Eng.*, vol. **26**, no. 2, pp. 218–230, 2004.

Judd, R. L., On nucleation site interaction, *J. Heat Transf.*, vol. **7110**, pp. 475–478, 1988.

Jung, Y. C. and Bushan, B., Dynamics effects of bouncing water droplets on superhydrophobic surfaces, *Langmuir*, vol. **24**, pp. 6262–6269, 2008.

Kandlikar, S. G. and Steinke, M. E., Contact angles of droplets during spread and recoil after impinging on a heated surface, *Trans. IChemE.*, vol. **79**, pp. 491–498, 2001.

Marmur, A., Measures of wettability of solid surfaces, *Euro. Phys. J. Special Topics*, vol. **197**, no. 1, pp. 193–198, 2011.

McHale, J. P. and Garimella, S. V., Bubble nucleation characteristics in pool boiling of a wetting liquid on smooth and rough surfaces, *Int. J. Multiphase Flow*, vol. **36**, pp. 249–260, 2010.

Moita, A. S. and Moreira, A. L. N., Influence of surface properties on the dynamic behaviour of impacting droplets, *Proc. of the 9th Intl. Conf. on Liquid Atomization and Spray Systems*, Sorrento, Italy, July 13–17, 2003.

Moita, A. S. and Moreira, A. L. N., Scaling the effects of surface topography in the secondary atomization resulting from droplet/wall interactions, *Exp. Fluids*, vol. **52**, no. 3, pp. 679–695, 2012.

Moita, A. S., Teodori, E., and Moreira, A. L. N., Enhancement of pool boiling heat transfer by surface micro-structuring, *J. Phys.: Conf. Series*, vol. **395**, paper 012175, 2012.

Moita, A. S., Teodori, E., and Moreira, A. L. N., Effect of surface topography in the boiling mechanisms, *Int. J. Heat Fluid Flow*, vol. **52**, pp. 50–63, 2015.

Moreira, A. L. N., Multi-scale interfacial phenomena and heat transfer enhancement, *Proc. of the 14th IHT*, Kyoto, Japan, August 10–15, 2014.

Mudawar, I. and Anderson, T. M., Parametric investigation into the effects of pressure, subcooIing surface augmentation and choice of coolant on pool boiling in the design of cooling systems for high-power-density electronic chips, *J. Electron Packag.*, vol. **112**, pp. 375–382, 1990.

Nitesh, D., Nimkar, S., Bhavnani, H., and Jaeger, R. C., Effect of nucleation site spacing on the pool boiling characteristics of a structured surface, *Int. J. Heat Mass Transf.*, vol. **49**, pp. 2829–2839, 2006.

Pina, H., Métodos numéricos, Editora McGraw-Hill de Portugal, Lisbon, 1995.

Pioro, I. L., Experimental evaluation of constants for the Rohsenow pool boiling correlation, *Int. J. Heat Mass Transf.*, vol. **40**, pp. 2379–2392, 1999.

Rohsenow, W. M., A method of correlating heat transfer data for surface boiling of liquids, *Trans. ASME*, vol. **74**, pp. 969–976, 1952.

Sauer, Jr. H. J., Medrow, R. A., and Sinnarwalla, A. M., Effects of surface condition on nucleate boiling of refrigerant-11, *ASHRAE Trans.*, vol. **81** (Pt. 2), pp. 274–281, 1975.

Stephan, K. and Abdelsalam, M., Heat-transfer correlations for natural convection boiling, *Int. J. Heat Mass Transf.*, vol. **23**, pp. 73–87, 1980.

Teodori, E., Moita, A. S., and Moreira, A. L. N., Characterization of pool boiling mechanisms over micro-patterned surfaces using PIV, *Int. J. Heat Mass Transf.*, vol. **66**, pp. 261–270, 2013.

Teodori, E., Moita, A. S., and Moreira, A. L. N., Empirical correlations between bubble dynamics and heat transfer coefficient for pool boiling over micro-textured surfaces, *Proc. of the 17th Int. Symposium on Laser Techniques Applied to Fluid Mechanics*, Lisbon, Portugal, July 7–10, 2014.

Tien, C. L., A hydrodynamic model for nucleate pool boiling, *Int. J. Heat Mass Transf.*, vol. **5**, pp. 533–540, 1962.

Vachon, R. I., Nix, G. H., and Tanger, G. E., Evaluation of constants for the Rohsenow pool-boiling correlation, *ASME J. Heat Transfer*, vol. **90**, pp. 239–246, 1968.

Wenzel, R. N., Resistance of solid surfaces to wetting by water, *J. Ind. Eng. Chem.*, vol. **28**, no. 8, pp. 988–994, 1936.

Young, T., An essay on the cohesion of fluids, *Phil. Trans. R. Soc. Lond.*, vol. **95**, pp. 65–87, 1805.

Yu, C. K., Lu, D. C., and Tsung, C. C., Pool boiling heat transfer on artificial micro-cavity surfaces in dielectric fluid FC-72, *J. Micromech. Microeng.*, vol. **16**, pp. 2092–2099, 2006.

Zhang, L. and Shoji, M., Nucleation site interaction in pool boiling on the artificial surface, *Int. J. Heat Mass Transfer*, vol. **46**, pp. 513–522, 2003.

APPENDIX

This appendix provides a more comprehensive description of the formulation considered for devising the proposed correlations, as well as a description of how the fitting parameters were determined.

A new relation proposed here considers C_{sf}, as defined by Rohsenow, as a more complex function of surface topography:

$$C_{sf} = a \cdot \ln\left(\frac{L_c}{S} \cdot \frac{A_{en}}{A_{smooth}}\right) + b \tag{A1}$$

The mathematical function defined in Eq. (A1) was not deduced. Instead, it was the result of an exhaustive analysis of various possible functions that would fit the experimental data. Linear, exponential, and logarithmic functions were tested. The final correlation selected was the one providing the best fit to the data. The observed trend in the experimental data was accepted because it was in line with work reported in the literature and with our own experimental results. The devised function was then linearized and the fitting parameters were determined using the linear least-squares method. Several matrix decomposition procedures for the linear least-squares method were used to verify the quality of the fitting procedure: QR decomposition, Gram-Schmidt decomposition, singular value decomposition, and the MATLAB function Polyfit. Furthermore, a nonlinear least-squares method was applied and the results were compared to those obtained with the linearized function.

The new relation was introduced in the Rohsenhow correlation as follows:

$$\mathrm{St}^* = C_{sf} \cdot \mathrm{Re}_b^m \cdot \mathrm{Pr}^n \tag{A2}$$

after determining m and considering the following:

- C_{sf} is considered to be a function of the geometric parameter $[(L_c/S) \cdot (A_{en}/A_{smooth})]$, in agreement with the first fitting procedure.
- The value of n does not depend on the pressure, but, like C_{sf}, is considered to be a function of $[(L_c/S) \cdot (A_{en}/A_{smooth})]$; a modified Rohsenow correlation can be obtained that emphasizes the role of the surface properties:

$$\mathrm{St}^* = C \cdot \left[\frac{L_c}{S} \cdot \frac{A_{en}}{A_{smooth}} \right]^{a1} \cdot \mathrm{Re}_b^m \cdot \mathrm{Pr}^{a2 \cdot \left[\frac{L_c}{S} \cdot \frac{A_{en}}{A_{smooth}} \right]} \tag{A3}$$

To determine the fitting parameters of such complex power functions, a linearized version of the power function was used (and is recommended) as a first fitting approach (e.g., Pina, 1995):

$$\ln \mathrm{St}^* - m \cdot \ln \mathrm{Re}_b = a1 \cdot \ln \left[\frac{L_c}{S} \cdot \frac{A_{en}}{A_{smooth}} \right] + a2 \cdot \left[\frac{L_c}{S} \cdot \frac{A_{en}}{A_{smooth}} \right] \cdot \ln \mathrm{Pr} + C \tag{A4}$$

Then the fitting constants were determined using the MATLAB function lsqcurvefit. This function allows nonlinear curve-fitting problems to be solved with a least-squares method. The solution to the problem is based on the trust-region-reflective, or Levenberg-Marquardt, algorithm. In any case, the results obtained with the correlation in its power or logarithmic form were comparable in terms of quality of the fitting, as shown in the accompanying tables. The slight differences mainly relate to the approximations made when expressing the formulation in the logarithmic form (Pina, 1995). This procedure was followed throughout the entire study, but only the logarithmic form was reported for the sake of simplicity.
Logarithmic form:

	HFE 7000	**FC 72**	**Ethanol**	**Water**
$a(1)$	–2.3631	–1.0672	–1.1331	–2.0282
$a(2)$	0.4201	0.0538	0.0651	0.6959
C	–1.9813	–1.5497	–2.0077	–3.0568
max (Res)	0.1857	0.3742	0.1376	0.2534
Res_norm	1.7992	5.4429	0.7095	4.7509
R^2	0.9705	0.9404	0.9783	0.9239

Power form:

	HFE 7000	**FC 72**	**Ethanol**	**Water**
$a(1)$	–2.7068	–1.1551	–0.9879	–1.3696
$a(2)$	0.5144	0.0606	0.0384	0.2454
C	0.1177	0.2187	0.1379	0.0521
max (Res)	0.0363	0.0666	0.0098	0.0066
Res_norm	0.0455	0.3457	0.0034	0.0036
R^2	0.9885	0.8699	0.9811	0.9049

Fitting constants in Eqs. (18) and (23) were also determined using the function lsqcurvefit. However, in this case the power form of the correlation was chosen instead of the logarithmic form because it made it easier to identify the important groups and relate them to the actual heat transfer processes under discussion.